Supplementary Information

Biogenic Manganese Oxide: Effective New Catalyst for Direct Bromination of Hydrocarbons

Yuta Nishina,* Hideki Hashimoto,* Noriyasu Kimura, Naoyuki Miyata, Tatsuo Fujii, Bunsho Ohtani and Jun Takada

Table of contents

Methods

Cultivation of Mn-oxidizing microorganisms Mn-oxidizing enrichment culture obtained from a riverbed biofilm[24,25 in the main text] was used for the production of BMO. The enrichment culture consisted of a microbial community including diverse Mn-oxidizing bacteria[27 in the main text]. Repeated batch cultivation was performed in a 35-L porypropylen vessel at ambient temperature under unsterilized conditions. The vessel was filled with 20 L of a basal medium containing (per litre of tap water) 200 mg $CH_3COONa{\cdot}3H_2O$, 80 mg soy peptone and 20 mg KH_2PO_4. The enrichment culture was inoculated into the vessel, then stock solution of $MnSO_4$ was added to obtain a dissolved Mn^{2+} concentration of 5 mg/L and finally the vessel was aerated at a flow rate of 4 L/min. After the first round of cultivation (3.5 days), the obtained suspended solid was left to stand for 180 min, supernatant was removed, the vessel was filled with fresh Mn^{2+} medium (5 mg/L) and 3-times-repeated batch cultivation was continued. After the subsequent rounds of cultivation (3.5 days per round), these steps were repeated, but with 4-times-diluted basal medium of the same Mn^{2+} concentration. Cultivation was considered complete when sufficient black precipitate for our needs had been produced on the vessel's bottom and wall (Figures S6a–b). The concentration of dissolved Mn in the cultures was monitored in the supernatants by a colorimetric method with potassium

periodate. After confirming that >95% of the initial dissolved Mn^{2+} had been removed, stock solution of $MnSO_4$ was added to achieve a Mn^{2+} concentration of 5 mg/L. The obtained precipitate was washed with distilled water and vacuum dried (Figure S6c).

SEM measurements SEM measurements were performed on SEM (Hitachi S-4300 and JEOL JSM-6700FE). Sample powder was coated with evaporated platinum.

STEM and TEM measurements STEM, TEM and HAADF-STEM images were collected from sample powder dispersed on a carbon-coated copper grid. Cross-sectional measurements were performed on ultrathin samples cut out by ultramicrotome. A STEM microscope (JEOL JEM-2100F) equipped with a CEOS spherical aberration corrector (C_s-corrector) was operated at an acceleration voltage of 200 kV.

Nitrogen-adsorption isotherm analysis Nitrogen-adsorption isotherms were measured at 77 K (BEL Japan Belsorp-mini II). Before measuring, samples were degassed under vacuum for 1 h at 120 °C and then for 4 h at 150 °C. Data analysis was performed by the Brunauer–Emmet–Teller (BET) method[30] for surface area and the Dollimore–Heal (DH) method[31,32] for pore size distribution.

EDX measurements EDX measurements were performed on an SEM (JEOL JSM-6700FE) equipped with an energy-dispersive X-ray analyser (JEOL JED-2200F). The atomic ratio of Mn:Ca:Mg:P:Al:Si:S:Cl (at%) was determined. Elemental mapping was done with an STEM (JEOL JEM-2100F) equipped with an energy-dispersive X-ray spectrometer (JEOL JED-2300T).

XRD measurements X-ray diffraction patterns were obtained on an X-ray powder diffractometer (Rigaku RINT-2000) using Cu Kα radiation.

XAFS measurements XAFS data were collected using beamline BL9C at the Photon Factory (IMMS, KEK, Tsukuba, Japan). Commercially available MnO_2 and Mn_2O_3 were measured as standard samples. Data were analysed with the Athena software program[33,34].

NMR measurements NMR spectra were recorded using a JEOL JNM-LA400 spectrometer. Proton chemical shifts are relative to solvent peaks [chloroform: 7.27 (^{1}H), 77.00 (^{13}C)]. The NMR spectra of organobromides **1′**, **1″**, **2′**, **2″**, **3′**, **4′**, **5′**, and **6′** showed complete agreement with the known data.

Preparation of reference samples MnO_2 with a large specific surface area (115 m^2/g) was synthesized by pouring a solution (2.2 ml) of 2.2 mmol $KMnO_4$ heated at 55 °C

into a solution (1.3 ml) containing 3.3 mmol $MnSO_4$ and 3.3 mmol H_2SO_4 under stirring at 55 °C. The obtained suspension was aged for 1 h at 90 °C, filtered, washed with distilled water and air-dried at 110 °C for 20 h.

Low-crystalline Na-birnessite was prepared by quickly pouring a solution (200 ml) of 1M H_2O_2 and 0.6M NaOH into a solution (100 ml) of 0.3M $Mn(NO_3)_2$, then stirring rapidly at room temperature for 10 min. The reaction was completed immediately and a black–brown suspension was obtained. The obtained suspension was aged for 1 day at 60 °C, filtered, washed with distilled water and vacuum dried.

Mn oxide with a chemical composition similar to that of BMO was prepared as follows. MnO_2 (99.99%, Kojundo Chemical Laboratory Co., Ltd.), $CaCO_3$ (99.99%, Kanto Chemical Co., Inc.), $Ca(H_2PO_4)_2{\cdot}H_2O$ (90.0%, Nacalai Tesque, Inc.), KCl (99.5%, Kanto Chemical Co., Inc.), SiO_2 (Aerosil®, 97.87%, Nippon Aerosil Co., Ltd.), $Al_2(SO_4)_3{\cdot}8H_2O$ (100%, Nacalai Tesque, Inc.) and $MgCl_2{\cdot}6H_2O$ (98.0%, Nacalai Tesque, Inc.) were weighted by imitating the chemical composition of BMO as described above, and then mixed with an alumina mortar. The resulting powder was pelletized at a pressure of 1000 kg/cm^2, heated at 400 °C for 2 h and crushed to a fine powder. The chemical composition was determined to be Mn:Ca:K:Cl:S:P:Si:Al:Mg = 89.1:4.3:0.3:1.3:1.0:1.6:1.0:0.4:1.0, nearly equal to that of BMO.

The catalytic performances of the above samples were measured under the same conditions as for BMO.

S1 Pore size distribution

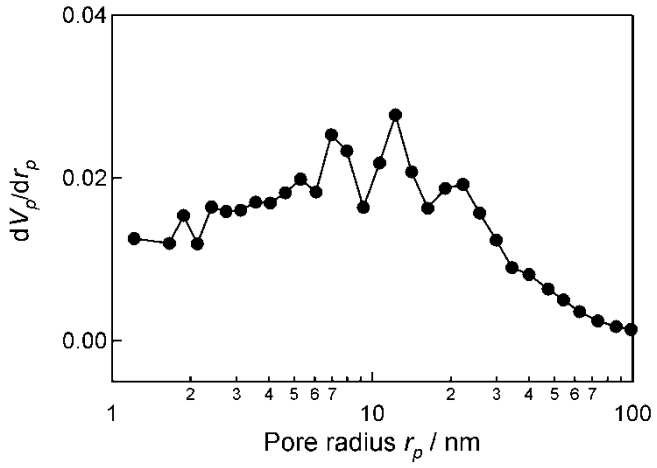

Figure S1. Pore size distribution for BMO, calculated by the DH method from nitrogen-adsorption isotherms. Pores are broadly distributed in the mesopore region r_p = 1–100 nm. They most probably correspond to the irregular open channels in the spongy structure of BMO and the multiple steps on the surface of BMO nanosheets, observed in the HAADF-STEM and TEM images of Figures 1g and f, respectively.

S2 Crystal structure

Crystal structure analysis of BMO was performed with XRD measurements and TEM-ED. It is commonly accepted that the crystal structure of biogenic manganese oxides resembles that of birnessite (with layer structure) or todorokite (with tunnel structure), consisting of edge-sharing MnO_6 octahedral sheets[35-38]. Crystal structure models of Na-birnessite and Mg-todorokite are shown in Figure S2. Na^+ and Mg^{2+} exist as interlayer and in-tunnel ions, respectively. We prepared Na-birnessite and Mg-todorokite as reference samples according to the reports of Feng *et al.*[28] and Yang *et al.*[39], respectively. Typical XRD pattern of BMO and the reference samples are shown in Figure S3a; *d*-spacing values and the associated Miller indexes (*hkl*) of their diffraction peaks are shown in Figure S3(B). Bragg diffractions with *d*-spacing values of 0.957 and 0.483 nm, suggesting a layer and/or tunnel structure of (001) and (002) planes, is observed in the XRD pattern of BMO. Diffraction peaks with *d*-spacing values of 0.25 and 0.14 nm correspond to (20*l*) and/or (11*l*) and (02*l*) and/or (31*l*) planes, respectively, indicating that BMO has edge-sharing MnO_6 octahedral sheets.

To obtain more detailed structural information, we performed TEM-ED measurements. Diffraction rings with *d*-spacing values of 0.248 and 0.145 nm are observed in the ED pattern of a BMO nanosheet (Figure S3). These diffractions

correspond to in-plane diffractions of (20*l*) and/or (11*l*) and (02*l*) and/or (31l), respectively, while interlayer diffraction of (001) and (002) are not observed. These results indicate that BMO nanosheet corresponds to edge-sharing MnO_6 octahedral sheet (in-plane is *ab* plane), and MnO_6 octahedral sheets are stacked to 00*l* direction. Diffractions of (*h*00) planes being attributed to a tunnel structure are not observed in the ED pattern, indicating that the crystal structure of BMO is layered birnessite-like structure.

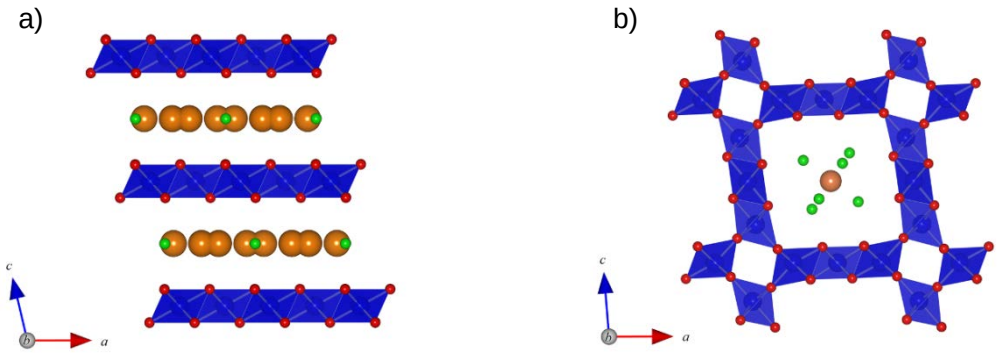

Figure S2. Crystal structure models of Na-birnessite and Mg-todorokite. Blue polyhedra represent MnO_6 octahedral units. Blue, red, green, large, and small ochre balls represent manganese, oxygen, water, sodium and magnesium, respectively. (a) Na-birnessite[40] with a layer structure of edge-sharing MnO_6 octahedral sheets. (b)

Mg-todorokite[41] with a [3×3] tunnel structure of edge-sharing MnO_6 octahedral sheets.

a)

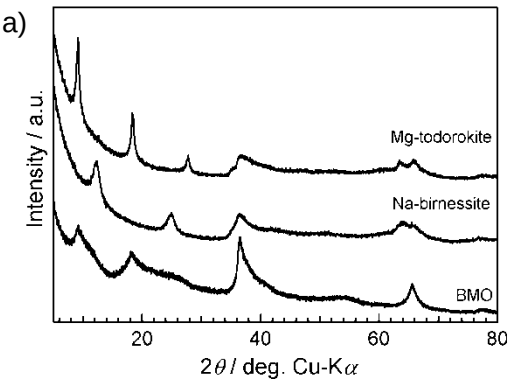

c)

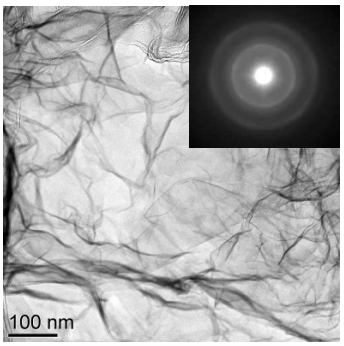

b)

	2θ/°	d/nm	2θ/°	d/nm	2θ/°	d/nm	2θ/°	d/nm	2θ/°	d/nm
BMO	9.23	0.957	18.36	0.483	-	-	36.61	0.245	65.60	0.142
Birnessite	12.27	0.721	24.84	0.358	-	-	36.60	0.245	63.87 66.06	0.146 0.141
Todorokite	9.15	0.965	18.39	0.482	27.72	0.322	35.85 36.92	0.250 0.243	63.59 65.87	0.146 0.142
hkl	001		002		003		20*l*, 11*l*		02*l*, 31*l*	

Figure S3. Crystal structure analysis of BMO. (a) Typical XRD pattern for BMO. Synthetic Na-birnessite and Mg-todorokite are also measured as reference samples. (b) 2θ and d-spacing values of the observed diffraction peaks and the associated Miller indexes. (c) TEM image of a BMO nanosheet and its ED pattern. The two rings of the ED pattern correspond to d-spacing values of 0.248 and 0.145 nm, which are nearly consistent with (20*l*) and/or (11*l*) and (02*l*) and/or (31*l*) planes, respectively.

S3 Elemental distribution

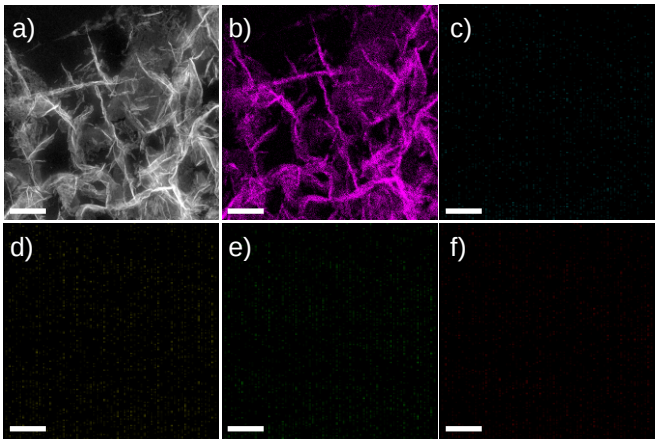

Figure S4. Elemental distribution of BMO. (a) STEM image of a sectioned hollow globule wall using high-angle annular dark-field (HAADF) detector and EDX imaging (spatial resolution, 1.2 nm) for Mn, Ca, Cl, P and Mg (b–f) taken from **(**a**)**. Bar, 100 nm.

S4 Average oxidation state and local structure

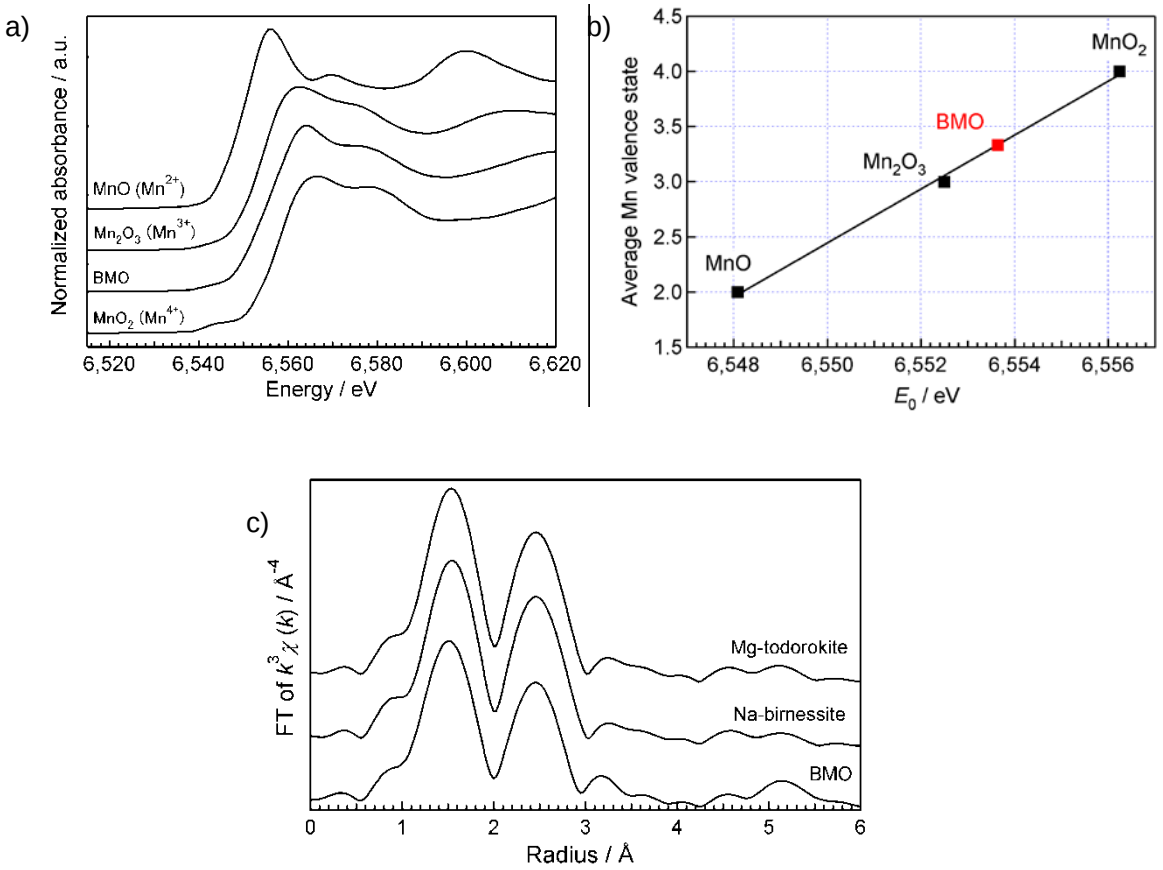

Figure S5. Mn K-edge XAFS results. (a) X-ray absorption near-edge-structure (XANES) spectra of BMO and standard samples, $Mn^{2+}O$, $Mn^{3+}{}_2O_3$ and $Mn^{4+}O_2$. The Mn K-edge absorption energy E_0 is located between $Mn^{3+}{}_2O_3$ and $Mn^{4+}O_2$. (b) The average Mn oxidation state of BMO (+3.3) is determined by calibration of X-ray absorption edge energies (E_0) against spectra collected from $Mn^{2+}O$, $Mn^{3+}{}_2O_3$, and $Mn^{4+}O_2$. (c) The radial structural functions (RSFs) of BMO, Na-birnessite and Mg-todorokite, derived by Fourier transformation of XAFS vibrations. The first and second peaks represent the correlation of Mn–O and Mn–Mn, respectively. All RSF

shapes are similar to each other, suggesting that all samples have a similar local structure of MnO_6 octahedra as primary units, which are consistent with XRD results.

S5 Culture vessels

Figure S6. Photos of the culture vessels used in this study. (a) The right-hand vessel (volume 35 *l*) with transparent tubes for aeration was used in this study. (b) Vessel interior with black BMO precipitate attached to the wall and bottom. (c) Dried BMO powder.

S6 Bromination of cyclohexane with other reagents

To compare the catalytic reactivity of BMO, known reagents and catalyst were investigated.

Table S1. Bromination of cyclohexane.

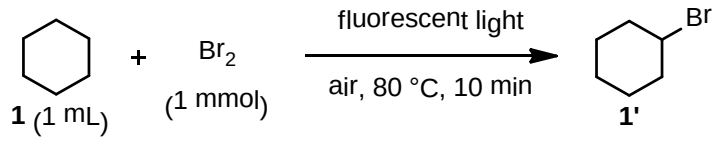

entry	additive or catalyst	yield /%
1[a]	AcOH (excess)	13
2[b]	^{t}BuONa (1 mmol)	35
3[c]	2AlBr$_3$/CBr$_4$ (0.08 mmol)	59
4[d]	MnO$_2$ (2 mmol)	77

a: In ref *42*, the reaction was performed for 24 h and gave **1′** in 13% yield. **b**: in ref *43*, the reaction was performed at 40 ˚C for 15 h and gave **1′** in 100% yield. **c**: The polyhalogenation occurred in this reaction condition. In ref *44*, the reaction was performed at -20 ˚C for 1 h and gave **1′** in 75% yield. **d**: In ref *45*, **1′** was obtained in 100% yield.

S7 Monochromatic irradiation-action spectrum analysis

We speculated that formation of one molecule of bromocyclohexane (**1′**) requires one photon, and formation of one molecule of dibromocyclohexane (**1′′**) requires two photons.

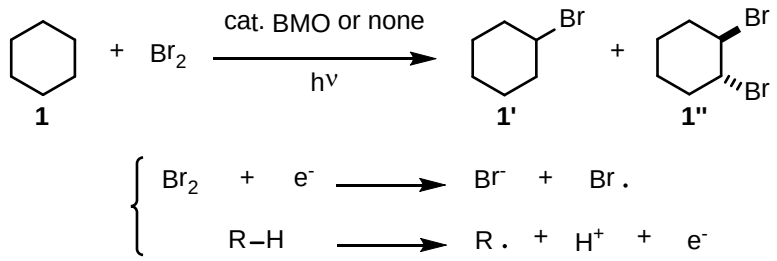

We measured light intensity at various wavelengths with an optical power meter (HIOKI Optical Power Meter 3664). We measured the numbers of product molecules **1′** and **1′′** with a gas chromatography (Shimadzu GC-2014) using dodecane as an internal standard. Detailed analysis data were shown in Table S2.

Table S2. Calculation of apparent quantum efficiency. (**A**) and (**B**) Reactions were performed in the presence of BMO (two runs). (**C**) Average apparent quantum efficiency based on the two runs. (**D**) Reactions were performed in the absence of BMO.

(A) With BMO (run 1)

Wavelength /nm	Light intensity/W	Numbers of irradiated photon/s	Numbers of product molecule/s		Number of used photon/s	Apparent quantum efficiency
			1'	1"		
320	0.00989	1.59E + 16	3.73 E + 16	0.06 E + 16	3.84 E + 16	2.41
335	0.01245	2.10E + 16	6.34 E + 16	0.00E + 00	6.34 E + 16	3.02
365	0.01643	3.02 E + 16	5.85 E + 16	0.41 E + 16	6.68 E + 16	2.21
395	0.01563	3.10 E + 16	5.97 E + 16	0.39 E + 16	6.76 E + 16	2.18
425	0.01555	3.32 E + 16	5.12 E + 16	0.29 E + 16	5.70 E + 16	1.71
455	0.01745	3.99 E + 16	6.00 E + 16	0.42 E + 16	6.84 E + 16	1.71
485	0.01532	3.74 E + 16	3.73 E + 16	0.88 E + 16	3.91 E + 16	1.05
515	0.01406	3.64 E + 16	4.39 E + 16	0.26 E + 16	4.92 E + 16	1.35
545	0.01329	3.64 E + 16	4.27 E + 16	0.16 E + 16	4.59 E + 16	1.26

(B) With BMO (run 2)

Wavelength /nm	Light intensity/W	Numbers of irradiated photon/s	Numbers of product molecule/s		Number of used photon/s	Apparent quantum efficiency
			1'	1"		
320	0.00989	1.59 E + 16	3.56 E + 16	0.06 E + 16	3.66 E + 16	2.30
335	0.01245	2.10 E + 16	6.34 E + 16	0.23 E + 16	6.81 E + 16	3.25
365	0.01643	3.02 E + 16	6.67 E + 16	0.34 E + 16	7.35 E + 16	2.44
395	0.01563	3.10 E + 16	5.70 E + 16	0.34 E + 16	6.38 E + 16	2.28
425	0.01555	3.32 E + 16	4.89 E + 16	0.23 E + 16	5.34 E + 16	1.72
455	0.01745	3.99 E + 16	4.71 E + 16	0.40 E + 16	5.51 E + 16	1.76
485	0.01532	3.74 E + 16	3.78 E + 16	0.09 E + 16	3.97 E + 16	1.20
515	0.01406	3.64 E + 16	4.11 E + 16	0.26 E + 16	4.63 E + 16	1.37
545	0.01329	3.64 E + 16	4.38 E + 16	0.14 E + 16	4.65 E + 16	1.16

(C) Average of run 1 and 2

Wavelength/nm	Apparent quantum efficiency (average of runs 1 and 2)
320	2.37
335	3.15
365	2.34
395	2.24
425	1.73
455	1.75
485	1.13
515	1.37
545	1.22

(D) No catalyst

Wavelength /nm	Light intensity/W	Numbers of irradiated photon/s	Numbers of product molecule/s		Number of used photon/s	Apparent quantum efficiency
			1'	1"		
320	0.00989	1.59E + 16	0.50E + 15	0.04 E + 15	0.06E + 16	0.363
350	0.01387	2.44 E + 16	4.37 E + 15	1.00 E + 15	0.64 E + 16	0.261
380	0.01464	2.80 E + 16	7.77 E + 15	1.60 E + 15	1.10 E + 16	0.392
440	0.01532	3.39 E + 16	8.06 E + 15	1.59 E + 15	1.12 E + 16	0.331
500	0.01473	3.70 E + 16	8.38 E + 15	1.67 E + 15	1.17 E + 16	0.316
560	0.01066	3.00E + 19	5.48 E + 15	1.29 E + 15	0.81 E + 16	0.269

References and Notes

31. S. Brunauer, P. H. Emmett, E.Teller, *J. Amer. Chem. Soc.* **60,** 309 (1938).

32. D. Dollimore, G. R. Heal, *J. Applied Chem.* **14**, 109 (1964).

33. D. Dollimore, G. R. Heal, *J. Colloid Interface Sci.* **33**, 508 (1970).

34. B. Ravel, M. Newville, *J. Synchrotron Rad.* **12**, 537 (2005).

35. M. Newville, *J. Synchrotron Rad.* **8**, 322 (2001).

36. I. Saratovsky *et al*., *J. Amer. Chem. Soc.* **128**, 11188 (2006).

37. I. Saratovsky, S. J. Gurr, M. A. Hayward, *Geochim. Cosmochim. Acta* **73**, 3291 (2009).

38. V. Petkov *et al*., *ACS nano* **3**, 441 (2009).

39. S. Grangeon, B. Lanson, N. Miyata, Y. Tani, A. Manceau, *Am. Mineral.* **95**, 1608 (2010).

40. X. Yang, H. Kanoh, W.Tang, Z. H. Liu, K. Ooi, *Chem. Lett.* 1192 (2000).

41. J. E. Post, D. R. Veblen, *Am. Mineral.* **75**, 477 (1990).

42. J. F. Post, P. Heaney, J. Hanson, *Am. Mineral.* **88**, 142 (2003).

43. T. M. Shaikh, A. Sudalai, *Tetrahedron Lett.* **46**, 5587 (2005).

44. R. Montoro, T. Wirth, *Synthesis* **9**, 1473 (2005).

45. I. S. Akhrem, A. V. Orlinkov, L. V. Afanas'eva, E. I. Mysov, M. E. Vol'pin, *Tetrahedron Lett.* **36**, 9365 (1995).

46. X. Jiang, M. Shen, Y. Tang, C. Li, *Tetrahedron Lett.* **46**, 487 (2005).